

Flow Structures in Compact Plate Heat Exchangers: A Numerical Study with Experimental Validation

Caner Şenkal¹, Özgür Ertunç²

¹Research and Development Center, Bosch Termoteknik Isıtma ve Klima San. Tic. A.Ş.,
Manisa 45030, Turkey

²Department of Mechanical Engineering, Ozyegin University, 34794 Istanbul, Turkey

Corresponding author: caner.senkal@tr.bosch.com

Abstract: Flow structures generated by the corrugations of plate heat exchangers play a crucial role on its performance. In order to understand their influence by using simulations and optimize them numerically, the simulation models have to be calibrated. In the present work, industry standard RANS simulations are compared with flow visualization and pressure drop experiments. A grid independency study is made at various flow rates. Different turbulent eddy viscosity models are tested and compared against measurements. Flow structures found in experiments and simulations are shown.

Keywords: Flow Visualization, RANS Simulations, Compact Plate Heat Exchanger

1 Introduction

Due to their high thermal-hydraulic performances, compactness, high heat transfer efficiency and high rigidity, cross-corrugated plate heat exchangers (CC-PHEs) have been widely used in a broad range of industrial applications involving in heating, cooling, evaporation and condensation. The typical industries include automotive, beverage, chemical, dairy, HVAC, marine, metal and oil refinery, petroleum, pharmaceutical, power, district heating etc..

As there is a increasing demand of PHEs on the heat transfer equipment market, most of the investigations has focused on exploring the effects of geometric parameters, such as corrugation profile, corrugation inclination angle, corrugation pitch and height of those devices on the heat transfer and pressure drop. A good review is provided by Han *et al.* [1] A relatively sparse amount of study and investigation has been performed on visualizing complex channel flow phenomenon of PHEs. Focke and Knibbe [2] investigated flow patterns in ducts with corrugated walls by means of flow visualization

experiments. Chevron angles of plates, 0° , 45° , 80° , 90° relative to the duct axis were tested in their experiments. In the case of 45° , the flow was found to follow mainly the furrows of each wall and spirals in them. When the corrugations were at an angle of 80° , the flow does not follow a single furrow along the whole width of the plate, instead it is reflected close to contact points of the plates, a helical flow pattern resulted. In a numerical study, Sarraf, Launay and Tadrist [3] highlighted the relation between flow structures and friction coefficients in a brazed plate heat exchanger (BPHE) channel. From the two flow structures described in the literature, namely the “helical” and “cross-flows” types, flow phenomenon in BPHE channels were identified with the help of these quantities whether of these flow type is dominant. They reported that the flow structure types are not only sensitive to the chevron angle but also to the mass flow rate, and these two types of flow structure largely coexist within a certain range of Reynolds number (from 20 to 200).

Present study is dedicated to obtain deeper knowledge about the complex flow phenomenon taking place in a PHE, and its effect on hydraulic performance. Industry standard RANS simulations are conducted together with a qualitative technique of flow visualization in order to visualize and characterize the complex three-dimensional flow structure occurring in the corrugated channels. The simulated and measured pressure drop are compared with each other to reveal the accuracy of the numerical simulations.

2 Experimental Set-up

To reveal flow structures inside PHE channel, flow visualization experiments were carried out in a cross-corrugated hot water channel of a PHE (figure 1a). Two plates constitute one corrugated test channel. The channel geometry was upscaled 5 times. Water is used as the working fluid in experiments. The experiments are conducted around the operating Reynolds numbers of the real PHE. One side of each plate was turned via CNC while another side was kept unfinished. Test plates were fabricated from plexiglass material and corrugated surfaces were fine polished in order to obtain high transparency throughout the channel.

A schematic diagram of the experiment set-up is shown in Figure 2. A 300 lt water tank was used to store the water. Pump is used circulate the water. Flowrate is controlled by a ball valve. Outlet of the channel is open to atmosphere. Water flowrate, temperature and density was measured by a Coriolis flowmeter of Siemens – SITRANS series. The accuracy of this device is % 0.1 of the measured value. The pressure drop between the inlet and outlet ports of the PHE was measured with a differential an ABB pressure transducer. Pressure transducer has %0.075 of the measurement range 0-10 mbar. Very fine aluminum powder was used to visualize water flow throughout the domain. A high speed video camera (PHOTRON – miniUX series) is installed to the test rig to record flow structures inside the corrugated channel.

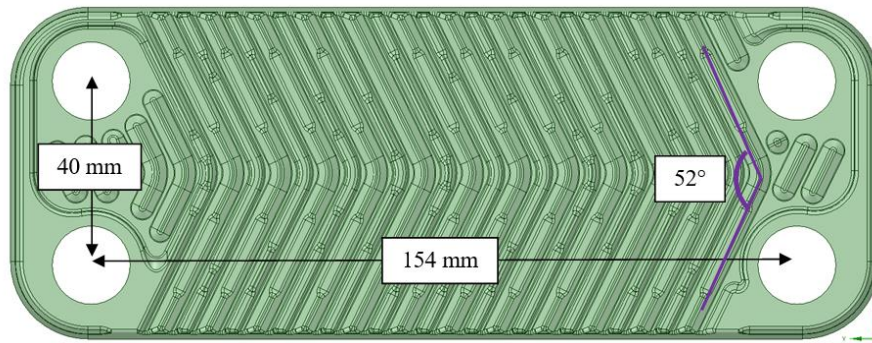
In the experiments, the Reynolds number in the channel varied between 207 to 1518. The channel Reynolds number is defined as follows;

$$Re = \frac{\rho \times u_c \times D_h}{\mu}$$

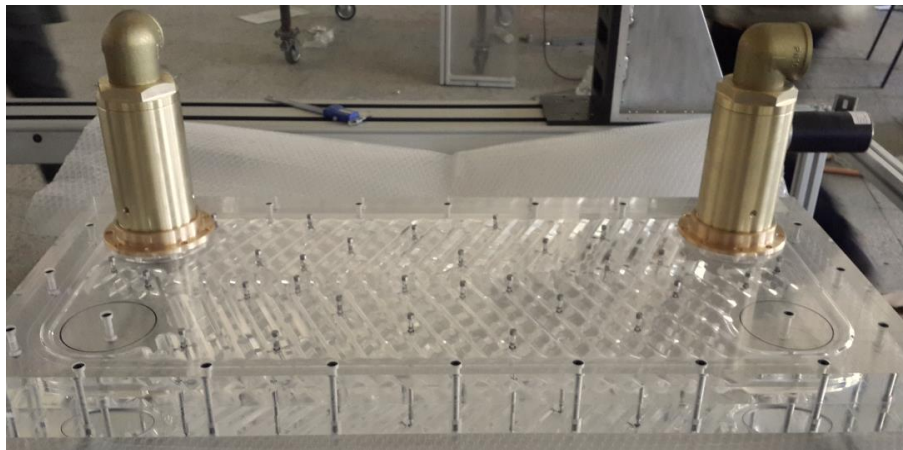
where u_c is the main velocity of water in the channel, D_h is the hydraulic diameter of the channel which corresponds to twice of the plate gap. In the cross corrugated channel the mean velocity u_c is defined by the flowrate G and the cross section area A_c of the channel, which can be described as; $u_c = G / A_c$. After the flow rate reaches to steady state, flow rate, temperature and pressure drop data were taken in 10 ms sampling interval for 60 seconds. Mean and standard deviation of pressure differences were calculated. Experiments were performed for different flowrates and the measured values from these experiments form the basis for validating and comparing to the results of CFD simulation. For quantitative comparison, the dimensionless representation of the energy losses, namely the friction coefficient of Darcy-Weisbach, is used:

$$f = \Delta P \times S^2 \times \left(\frac{D_h}{L}\right) \times 2 \times \left(\frac{\rho}{\dot{m}^2}\right)$$

where S is the cross sectional area of the channel, ΔP is the static pressure drop measured between inlet and outlet ports and obtained either from experiments or simulations.



(a)



(b)

Figure 1. (a) Fundamental dimensions of the hot water channel of a PHE (b) 5:1 upscaled Plexiglass model

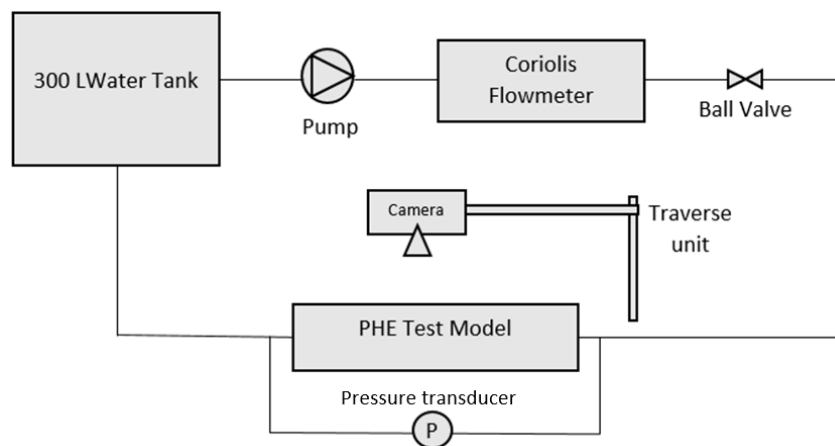


Figure 2. Test setup for flow visualization.

3 Numerical Set-up

The CFD software ANSYS Fluent was used to perform numerical simulations. The fluid flow field is represented in figure 3. The mesh of the simulated domain is composed of tetrahedral cells. One hot water channel of the PHE was taken into account in the simulations. A great effort was made to model fluid domain to obtain hot water channel geometry with real brazing point geometries. To achieve this, brazing points of a hot water channel of a PHE sample visually examined. Each geometrical feature of brazing points was modeled by means of investigating outline shapes of a sectional cut of a PHE sample.

“Inflation layer” near wall cells to resolve boundary layer could not be adopted in this study because total number of cells via inflation layers extremely increased computational resources. Figure 4a-b presents various sections including brazing points considered in the simulations.

The simulation boundary conditions are as follows:

- Inlet of the heat exchanger: Mass flow rate
- Outlet of the heat exchanger: imposed fluid pressure (open to the atmosphere)

Other faces of the fluid domain are set to wall boundary condition. Energy equation was not solved because only flow structures are under consideration in simulations.

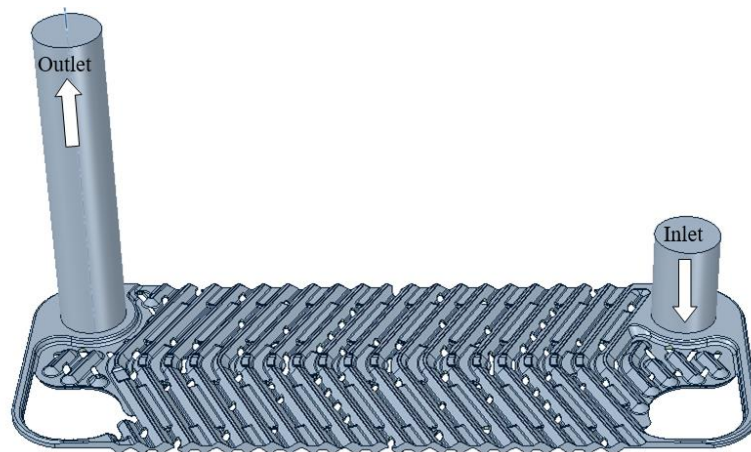


Figure 3. Flow domain

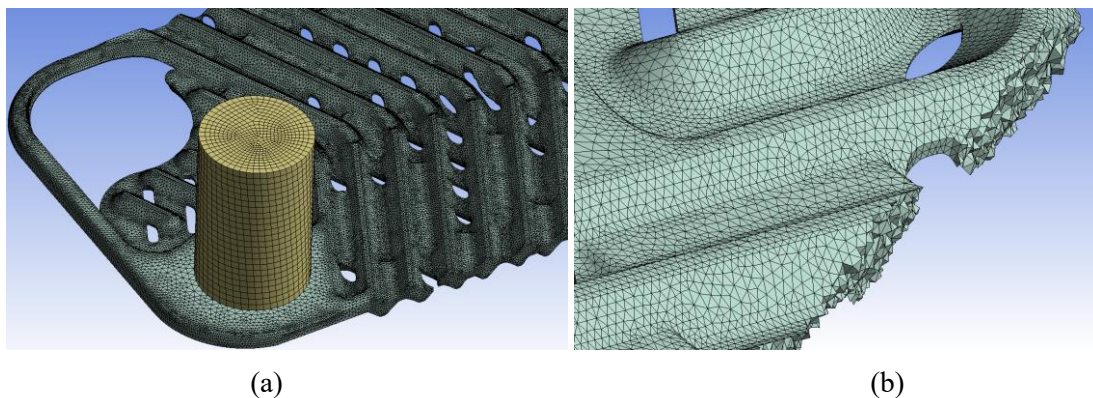


Figure 4. Computational grid used in simulations. (a) shows cells at the inlet port section, (b) shows cells at a brazing point section.

Grid independence was conducted (Figure 5). The pressure drop results showed that all models underestimate the measured pressure drop. The discrepancy increases with the increasing flow rate, i.e. increasing Reynolds number. Although, the accuracy improves with increasing number of cells, the improvement stagnates at about a base size of 0.3 mm in average which corresponds to circa 10 million cells.

The stagnation of the improvement suggests that it is not only the resolution but the turbulence models can be a reason for the discrepancy. Three turbulence models were tested with their standard settings: the $k-\epsilon$ turbulence model, $k-\omega$ standard and $k-\epsilon$ RNG models (see Figure 6). $k-\epsilon$ turbulence model was selected in simulations as it predicts the pressure drop closer to the measurements.

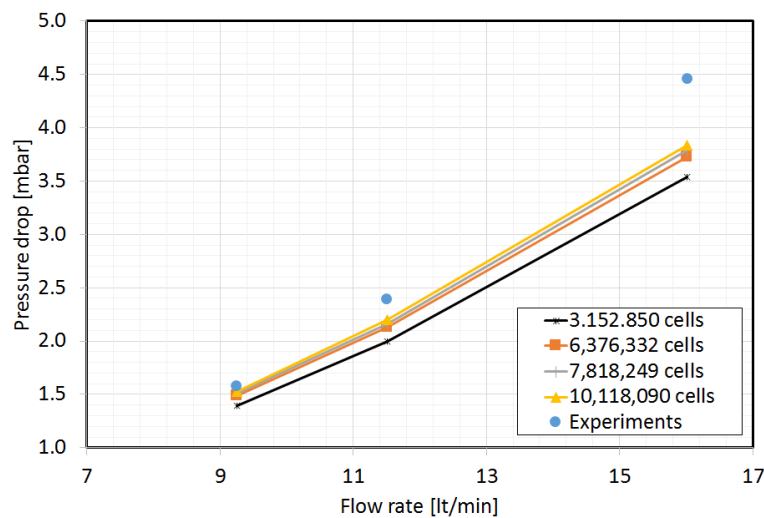


Figure 5. Dependency of pressure drop on the number of cells

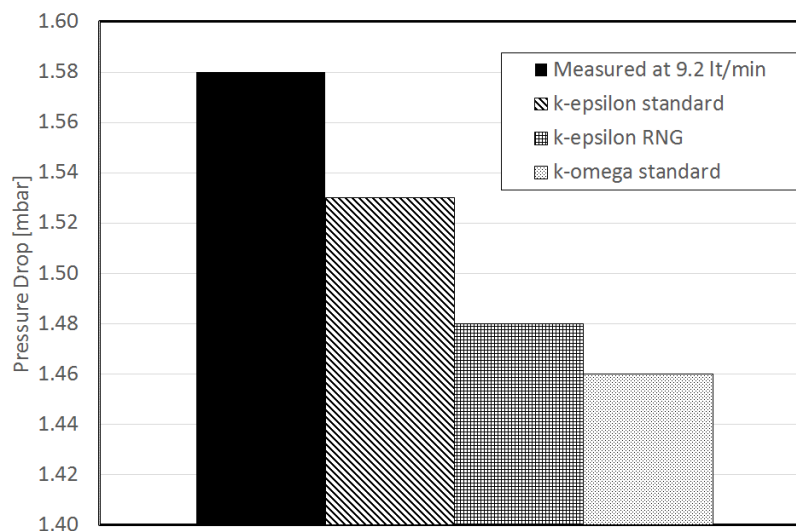


Figure 6. Dependency of pressure drop on the employed turbulence model

4 Results

4.1 Pressure drop

Simulations were conducted with the finest mesh with circa 10 million cells. The raw pressure drop-flow rate data from simulations and experiments are shown in Figure 7. Both data are well represented by power functions. In Figure 8, the dimensionless friction coefficients calculated from measured data reveals two distinct regimes. The regime regime is up to $Re < 750$ in which the friction coefficient can be represented well with a power curve. The second regime corresponds to $Re > 750$ and can be represented with a linear trend line. In contrary to experiments, the simulations depict continuous drop which can be well represented with a power function. As can be seen in Figure 9, the simulations over predict up to 10% at low Re and under predict with an increasing relative error in the second regime. Two regimes were also observed by Sarraf *et al.*[2] but at different Reynolds numbers since their geometry was different.

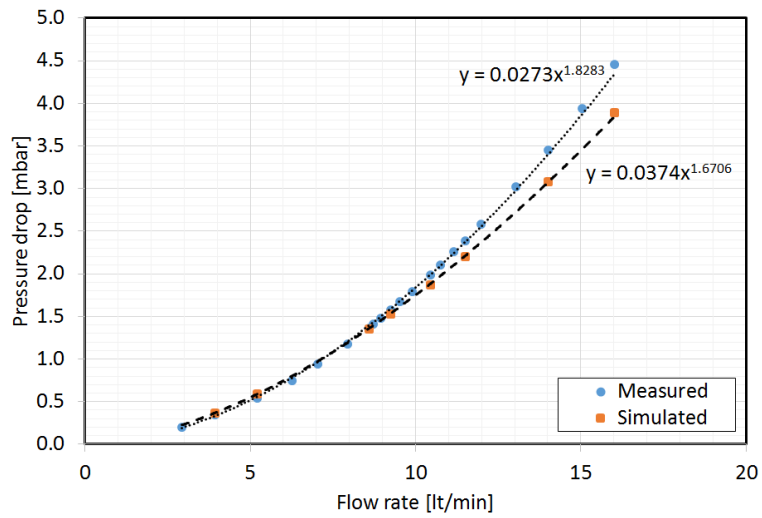


Figure 7. Measured and simulated pressure drop, lines show the trend lines

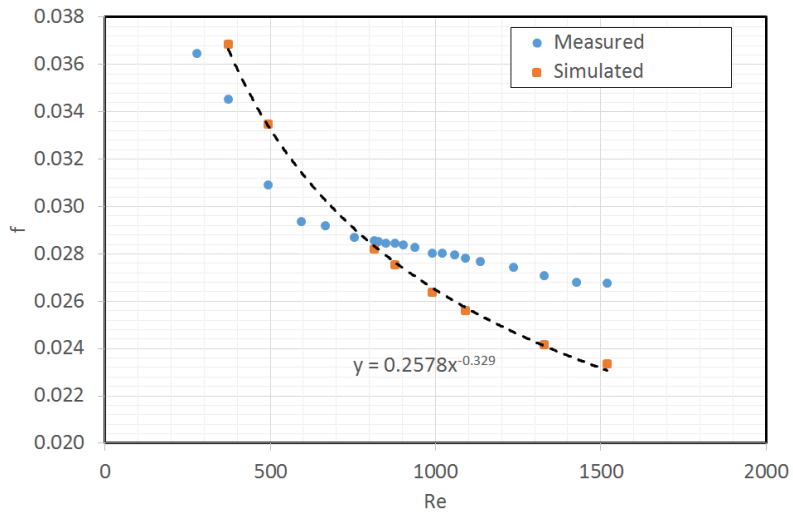


Figure 8. Measured and simulated friction coefficient

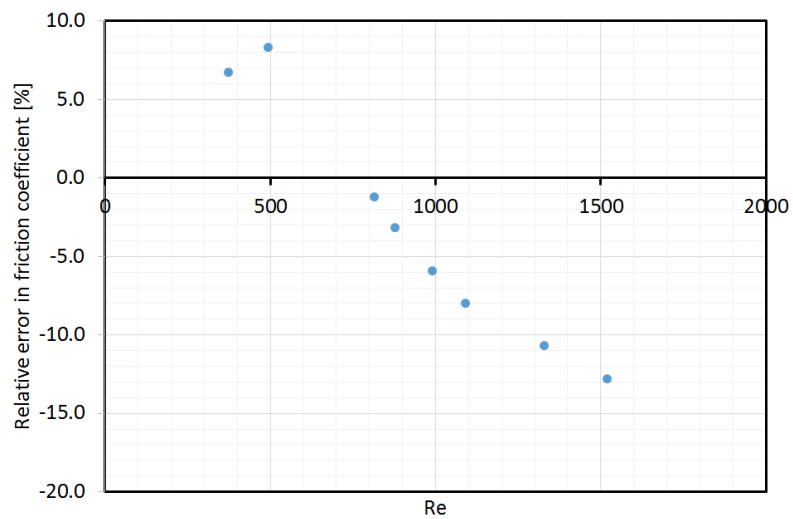


Figure 9. Relative deviation in friction coefficient between measurements and simulations

4.2 Flow structures

The flow structures in the simulations are analyzed at 9.2 lt/min ($Re=876$) where the discrepancy between experiments and the simulations is minimum. The numerical results were analyzed by inserting streamlines at three locations shown in Figure 10. At location A and B the flow blocked so extremely that recirculation regions occur (Figure 11a-b). Helical flow along the main flow direction was observed at all locations. At location A, an example of cross flow can be observed.

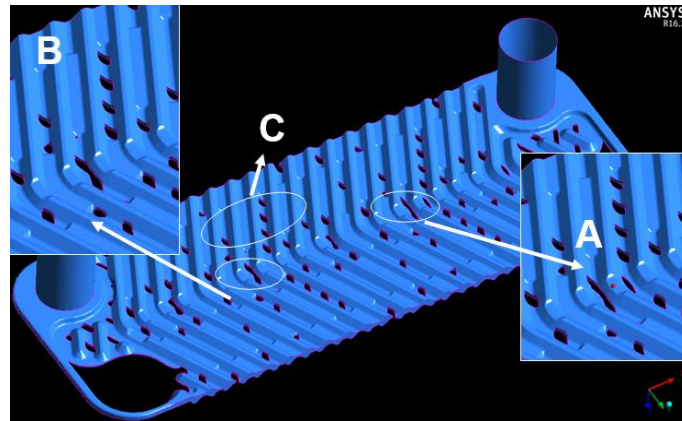
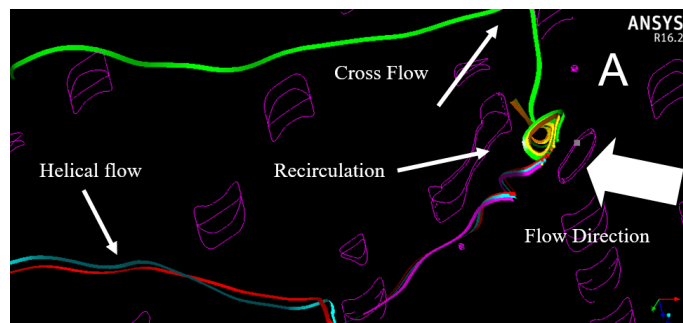
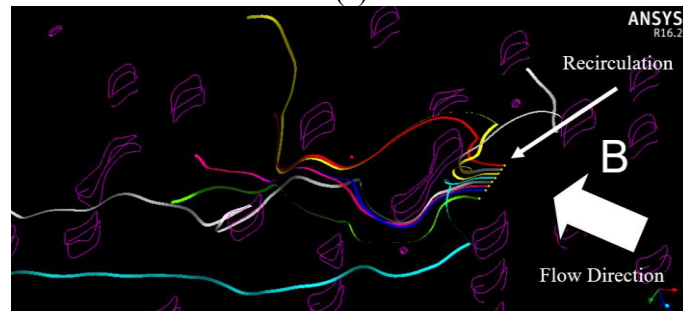


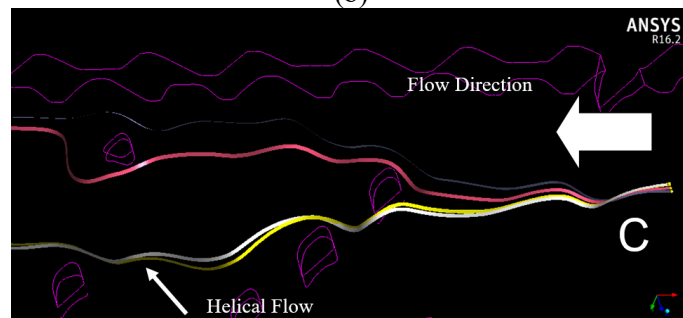
Figure 10. Analyzed locations for the flow structures



(a)



(b)



(c)

Figure 10 The flow structures observed at 9.2 lt/min ($Re=876$) (a) location A, (b) location B, (c) location C

The flow structures made visible with a laser sheet and aluminum particles. The high-speed image sequences were processed to obtain the visual impression of the flow field as shown in Figure 11a-c. In those images, the bright lines show the direction of the particles. The lines are short when the flow is too slow or it is out of the laser plane. The circulation region at the upstream of the brazing point (location A) is also observed in the experiments as can be seen in Figure 11a. At location C, the flow parallel to the flow and along one corrugation are shown in Figure 11b-c, respectively. As can be seen, there is strong interaction between the upper and lower corrugations. Most probably the flow along the corrugations are also helical.

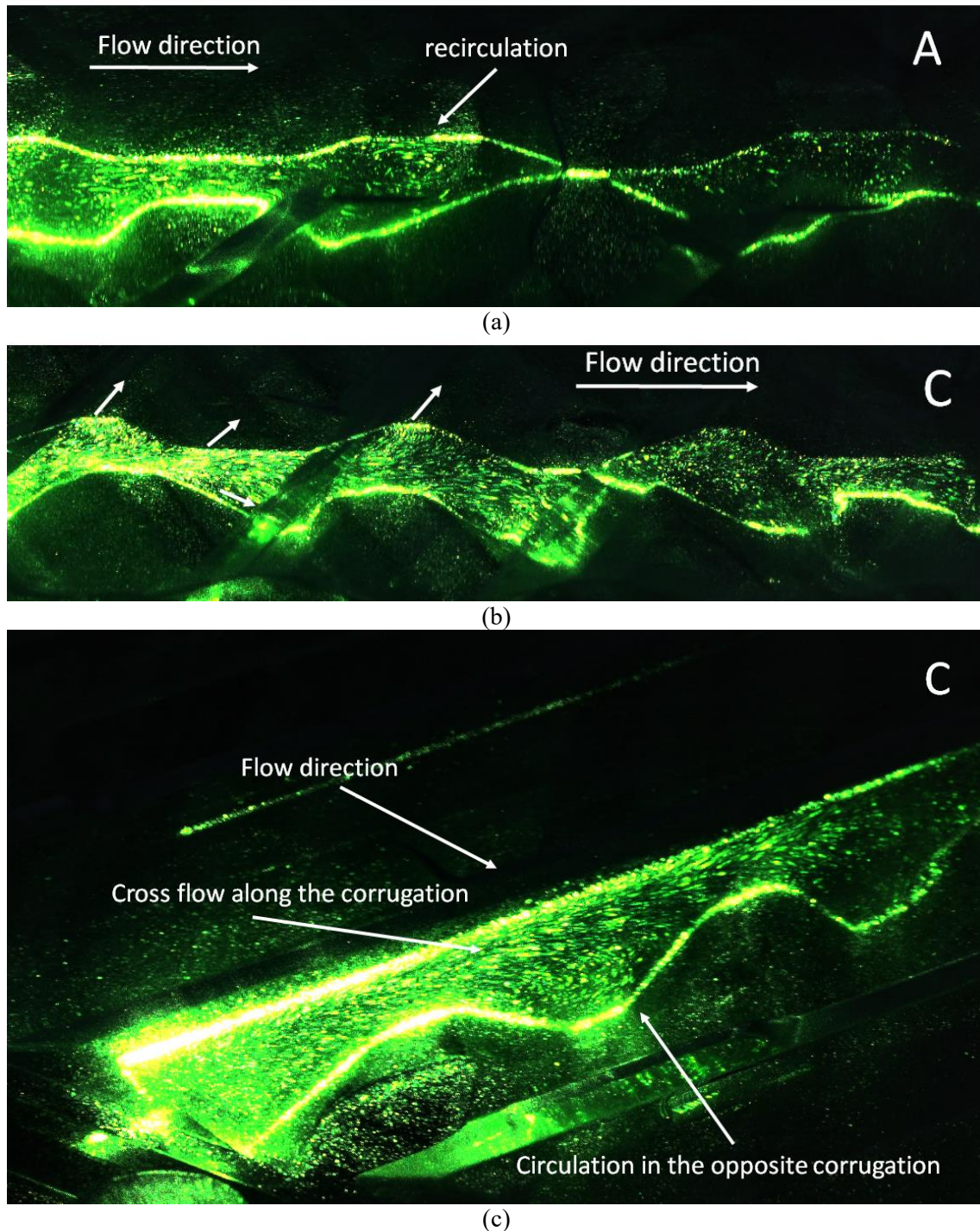


Figure 11. Flow structures in the PHE channel at 9.2 lt/min. (a) at location A just before the big brazing point (b) at location C along the main flow direction (c) at location C along one corrugation

5 Conclusion

The present work attempts to understand the flow phenomena and structures in a PHE both numerically and experimentally. The friction coefficient showed around 10 % discrepancy between the experiments and simulations. It is also shown that this discrepancy can be reduced neither by increasing the number of cells nor by using different types of eddy viscosity models.

Two distinct regimes were observed by looking to the friction coefficient as a function of Reynolds number. While the friction coefficient can be represented with a power curve at low Re, it shows a linear drop for $Re > 750$.

Visualization study was made at a flow rate having the minimum discrepancy. It was shown that helical, circulating and cross flow phenomena occur in the investigated PHE channel. Moreover, experimental visualization showed that cross flow along a corrugation can also be helical.

Acknowledgement

The authors would like to gratefully acknowledge Scientific and Technological Research Council of Turkey (TÜBİTAK) for providing financial support to this research with the TEYDEB 3150243 project.

References

- [1] W. Han, K. Saleh, V. Aute, G. Ding, Y. Hwang, and R. Radermacher, "Numerical simulation and optimization of single-phase turbulent flow in chevron-type plate heat exchanger with sinusoidal corrugations," *HVAC&R Res.*, vol. 17, no. 2, pp. 186–197, Apr. 2011.
- [2] W. W. Focke and P. G. Knibbe, "Flow visualization in parallel-plate ducts with corrugated walls," *J. Fluid Mech.*, vol. 165, pp. 73–77, Apr. 1986.
- [3] K. Sarraf, S. Launay, and L. Tadrist, "International Journal of Thermal Sciences Complex 3D-flow analysis and corrugation angle effect in plate heat exchangers," vol. 94, pp. 126–138, 2015.